Site-specific genome editing in *Plasmodium falciparum* using engineered zinc-finger nucleases

Judith Straimer[1], Marcus C S Lee[1], Andrew H Lee[1], Bryan Zeitler[2], April E Williams[3,4], Jocelynn R Pearl[2], Lei Zhang[2], Edward J Rebar[2], Philip D Gregory[2], Manuel Llinás[3,4], Fyodor D Urnov[2] & David A Fidock[1,5]

Malaria afflicts over 200 million people worldwide, and its most lethal etiologic agent, *Plasmodium falciparum*, is evolving to resist even the latest-generation therapeutics. Efficient tools for genome-directed investigations of *P. falciparum*-induced pathogenesis, including drug-resistance mechanisms, are clearly required. Here we report rapid and targeted genetic engineering of this parasite using zinc-finger nucleases (ZFNs) that produce a double-strand break in a user-defined locus and trigger homology-directed repair. Targeting an integrated *egfp* locus, we obtained gene-deletion parasites with unprecedented speed (2 weeks), both with and without direct selection. ZFNs engineered against the parasite gene *pfcrt*, responsible for escape under chloroquine treatment, rapidly produced parasites that carried either an allelic replacement or a panel of specified point mutations. This method will enable a diverse array of genome-editing approaches to interrogate this human pathogen.

© 2012 Nature America, Inc. All rights reserved.

By current estimates, 655,000 individuals die each year from severe malaria caused by the protozoan parasite *P. falciparum*. Recent reductions in the global disease burden, brought about by artemisinin-based combination therapies and anti-mosquito measures, are at risk of being overturned by mutation-driven resistance[1]. Defining molecular pathways of malaria pathogenesis and identifying mechanisms of treatment failure require precise manipulation of the parasite genome. Existing methods, despite having yielded important insights, do not adequately meet these challenges[2,3].

Genome editing with customized ZFNs has been successfully applied to a range of multicellular organisms[4,5]. To achieve editing, pairs of zinc-finger proteins with unique specificity for adjacent sequences on either strand of the DNA helix are linked to an endonuclease (FokI) that functions as an obligate heterodimer[6,7]. ZFNs induce a double-strand break (DSB) that can alter the target, either by activating the error-prone nonhomologous end-joining pathway or by stimulating homologous recombination when a donor template is provided. In metazoans, nonhomologous end joining can produce nuclease-mediated gene disruption[8]. However, *P. falciparum* lacks several critical components of this pathway (Ku70, Ku80 and DNA ligase IV[9]; unpublished observations). Thus, homologous recombination is likely the primary pathway of DSB repair in this parasite[10], and gene-targeting approaches using this process have been successful, albeit highly inefficient[3]. We hypothesized that ZFNs could improve efficiency by introducing DSBs in a specified target site at a much higher frequency than occurs stochastically. Here we establish methods of genome editing in *P. falciparum*.

RESULTS

2A peptide permits dual protein synthesis in *P. falciparum*

Directed genome editing requires the coordinated expression of two ZFNs that heterodimerize to cleave a unique site. Given the paucity of selectable markers for *P. falciparum* and the instability of propagating large plasmids containing AT-rich *P. falciparum* DNA in *Escherichia coli*[3], we first tested whether a plasmid-encoded ZFN pair could be coexpressed from a single promoter using a viral 2A 'ribosome skip' peptide. This short self-processing sequence permits polycistronic expression of individual polypeptides[11]. We generated transgenic parasites expressing a *mrfp*-2A-*gfp* fusion driven by the *calmodulin* promoter (**Fig. 1a**). Both protein products were detected in parasites by fluorescence microscopy, and immunoblotting for the downstream GFP reporter revealed its expression as the 27-kDa monomer (**Fig. 1a**). Deletion of a key proline residue in the 2A peptide crippled cotranslational release, resulting in a mRFP-2A$^{\Delta P}$-GFP fusion protein with a molecular mass slightly greater than the conventional fusion of these two proteins (**Fig. 1a**). These findings confirm efficient ribosomal skipping across the 2A site and illustrate its utility for dual protein expression from a single promoter in *P. falciparum*.

ZFNs mediate gene ablation in *P. falciparum* parasites

We set out to achieve ZFN-mediated gene disruption in *P. falciparum* by targeting a chromosomal *egfp* locus. First we integrated the target *egfp* gene into the *cg6* locus of NF54 parasites

[1]Department of Microbiology & Immunology, Columbia University College of Physicians and Surgeons, New York, New York, USA. [2]Sangamo BioSciences, Inc., Richmond, California, USA. [3]Department of Molecular Biology, Princeton University, Princeton, New Jersey, USA. [4]Lewis-Sigler Institute for Integrative Genomics, Princeton University, Princeton, New Jersey, USA. [5]Division of Infectious Diseases, Department of Medicine, Columbia University College of Physicians and Surgeons, New York, New York, USA. Correspondence should be addressed to D.A.F. (df2260@columbia.edu).

RECEIVED 22 MARCH; ACCEPTED 27 JULY; PUBLISHED ONLINE 26 AUGUST 2012; DOI:10.1038/NMETH.2143

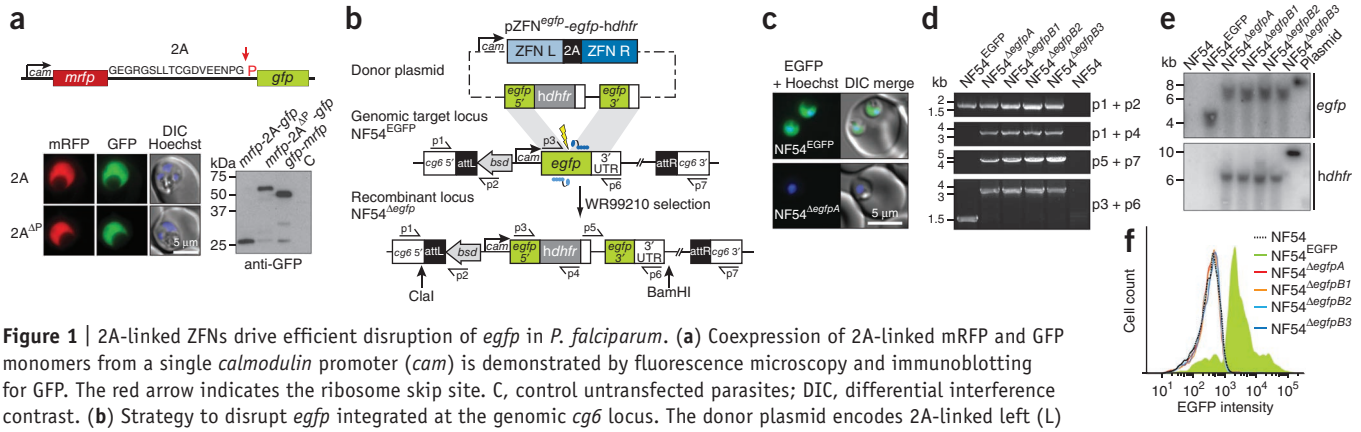

Figure 1 | 2A-linked ZFNs drive efficient disruption of *egfp* in *P. falciparum*. (**a**) Coexpression of 2A-linked mRFP and GFP monomers from a single *calmodulin* promoter (*cam*) is demonstrated by fluorescence microscopy and immunoblotting for GFP. The red arrow indicates the ribosome skip site. C, control untransfected parasites; DIC, differential interference contrast. (**b**) Strategy to disrupt *egfp* integrated at the genomic *cg6* locus. The donor plasmid encodes 2A-linked left (L) and right (R) ZFNs as well as *egfp* homologous regions flanking the ZFN target site (thunderbolt). Repair of the ZFN-induced DSB, via homology-directed repair using the donor as template, yielded an in-frame integration of h*dhfr* into the *egfp* locus. (**c**) Micrographs showing EGFP expression in the parental line NF54^{EGFP} but not in the recombinant line NF54$^{\Delta egfpA}$. Nuclei were stained with Hoechst 33342. (**d**) PCR analysis of the ZFN-transfected lines NF54$^{\Delta egfpA/B1/B2/B3}$ and the parental line NF54^{EGFP} using the primer (p) positions indicated in **b**. (**e**) Southern blot hybridization of genomic DNA digested with ClaI and BamHI (see **b**) demonstrates integration of h*dhfr* in the ZFN-transfected lines (bottom) and the expected 2-kb size increase at the disrupted *egfp* locus (top). (**f**) Flow cytometry reveals complete loss of EGFP signal in the ZFN-modified parasite populations.

using attB × attP integrase–mediated recombination[12], generating the NF54^{EGFP} line that was uniformly EGFP positive (**Fig. 1b–d**). We then designed a composite pZFN^{egfp}-*egfp*–human dihydrofolate reductase (h*dhfr*) donor plasmid comprising our 2A-linked *egfp*-specific ZFN expression cassette as well as two homology regions (*egfp* 5′ and 3′) that flanked the ZFN cleavage site. To select for *egfp*-disrupted parasites, the 5′ homology region was fused in frame with h*dhfr*[13] such that resistance to the antifolate drug WR99210 would be contingent on the *egfp*-h*dhfr* fusion integrating downstream of the genomic *calmodulin* promoter (**Fig. 1b**). Targeted integration of h*dhfr* into the *egfp* locus should produce a GFP-negative parasite.

After electroporation of the ZFN donor plasmid into the NF54^{EGFP} line, parasites were selected directly with WR99210 (yielding the NF54$^{\Delta egfpA}$ line) or first supplemented with red blood cells preloaded with plasmid DNA (reported to increase transformation efficiency[14] and yielding the three lines NF54$^{\Delta egfp\text{-}B1/B2/B3}$). With all four lines, WR99210-resistant parasites were detected 15 d after electroporation. We confirmed ZFN-driven disruption of the *egfp* gene by fluorescence microscopy, PCR and Southern blotting (**Fig. 1c–e**). Flow cytometry of the bulk cultures revealed the complete loss of fluorescence in all NF54$^{\Delta egfp}$ lines (**Fig. 1f**). Three independent transfections with a ZFN-deficient control p*egfp*-h*dhfr* plasmid failed to yield parasites after 60 d.

To assess potential off-target activity of the ZFNs, we sequenced the genomes of two edited lines (NF54$^{\Delta egfpA}$ and NF54$^{\Delta egpfB1}$) as well as the parent (NF54^{EGFP}). Sequence analysis revealed a depth of coverage of h*dhfr* (56× and 42× for NF54$^{\Delta egfpA}$ and NF54$^{\Delta egfpB1}$, respectively) that mirrored the average coverage across the entire genome (54× and 69×), consistent with the presence of a single genomic copy of h*dhfr* (**Supplementary Table 1**). Furthermore, flanking sequence reads that partially overlapped h*dhfr* could only be mapped to the *egfp*-h*dhfr* locus, consistent with the specific disruption of *egfp* (**Supplementary Fig. 1a,b**).

Gene replacement in the absence of a selectable phenotype

Gene disruption by in-frame integration of a selectable marker is limited to targets that are expressed during the asexual blood stage. We sought to develop a broader strategy for gene manipulation, irrespective of expression pattern during the parasite life cycle and independent of a selection event. We first aimed to replace the *egfp* reporter with monomeric *rfp* (*mrfp*) fused to the cytosolic ATPase *pfvps4*. This fusion was placed on a donor plasmid (p*mrfp-vps4*) flanked by *egfp* UTRs and plasmid backbone sequences (3.5 kb and 2.8 kb on the 5′ and 3′ ends, respectively) that provided templates for homologous recombination (**Fig. 2a**). ZFNs were expressed from a separate plasmid (pZFN^{egfp}-h*dhfr*) containing the h*dhfr* selectable marker. The plasmids were coelectroporated, and WR99210 pressure was applied for 6 d to transiently enrich for parasites that expressed the ZFNs. Parasite proliferation was detected microscopically 12 d after electroporation.

Imaging and quantification of parasite fluorescence from the bulk cultures was consistent with a gene replacement efficiency of 88% and 62% in two independent experiments (**Fig. 2b,c**). This level of efficiency was confirmed by analysis of clonal lines, which expressed mRFP and not EGFP in 19 of 27 (70%) and 21 of 39 (54%) cloned parasites from the two experiments. This recombination event involves DNA end resection of greater than 260 bp from at least one side of the DSB, leading to invasion of the *mrfp* flanking sequences common to both the donor plasmid and the chromosomal *egfp* locus (**Fig. 2a**). These flanking sequences were shared with the ZFN expression vector, which could compete with the p*mrfp-vps4* plasmid as a template for homology-directed repair and could account for the minority of nonfluorescent parasites observed in the bulk cultures (**Fig. 2c**). PCR and Southern blot analyses nonetheless confirmed replacement of *egfp* with the *mrfp* fusion in the majority of parasites, shown in two representative clones (**Fig. 2d,e**).

Allelic replacement of an endogenous parasite gene

An important drug-resistance determinant in *P. falciparum* is the chloroquine (CQ) resistance transporter PfCRT[15,16]. The extensive worldwide use of CQ in malaria treatment has led to the selection of multiple mutations in *pfcrt*[17]. Genetic engineering of isogenic parasites expressing various *pfcrt* alleles is required to fully analyze their phenotypic impact on drug response, but this has proven exceptionally time and labor intensive[18,19].

© 2012 Nature America, Inc. All rights reserved.

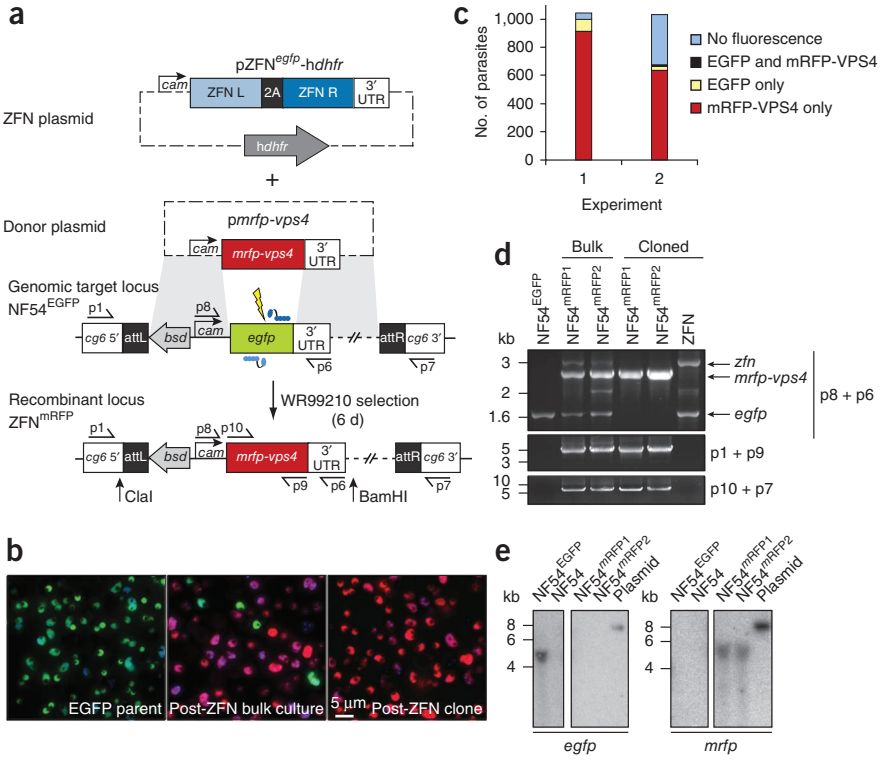

Figure 2 | ZFNs mediate efficient gene replacement of *egfp*. (**a**) Schematic of the *egfp* replacement strategy. ZFNs were expressed from the *calmodulin* promoter (*cam*) on the pZFN^{egfp}-h*dhfr* plasmid and were cotransfected with the *mrfp-vps4* donor sequence. Homology-directed repair of the ZFN-induced DSB, using the flanking regions on the donor as template, resulted in replacement of *egfp* with the *mrfp-vps4* fusion construct. (**b**) The parental line NF54^{EGFP}, a post-ZFN bulk culture and a clonal line were imaged for EGFP and mRFP expression. Nuclei were stained with Hoechst 33342. (**c**) Quantification of parasite fluorescence in the bulk culture in two independent experiments (n = 1,042 and n = 1,032). (**d**) PCR analysis of parental NF54^{EGFP} and ZFN-transfected bulk cultures and individual parasite clones. Primer (p) positions are shown in **a**. (**e**) Southern blot hybridization of genomic DNA from the indicated parasite lines digested with ClaI and BamHI (see **a**) using an *egfp* probe (left) and a *mrfp* probe (right). Linearized transfection plasmids served as positive controls.

We designed ZFNs against *pfcrt* using an archive of prevalidated modules, each consisting of two zinc fingers[8,20]. On the basis of results from yeast proxy cleavage assays[21] (data not shown), we selected the two most active nuclease pairs (13/15 and 14/15; **Supplementary Table 2**). These pairs, which target the boundary of intron 1 and exon 2, were cloned into a plasmid expressing a blasticidin S-deaminase (*bsd*) selectable marker, thereby yielding pZFN^{crt}-*bsd* (**Fig. 3a**). The *pfcrt* donor sequence was inserted on a second plasmid (p*crt*^{Dd2}-h*dhfr*), consisting of the *pfcrt* cDNA from the CQ-resistant (CQR) strain Dd2 and the 3′ UTR from the *P. berghei crt* ortholog, followed by an h*dhfr* expression cassette that served as an independent selectable marker. Upstream and downstream regions of homology flanked these elements to promote ZFN-mediated replacement of the entire 3.1-kb gene with the donor-provided *pfcrt* 1.2 kb-cDNA and the downstream h*dhfr* selectable marker (**Fig. 3a**).

We chose to modify the CQ-sensitive (CQS) strains 106/1 and GC03, which harbor distinct alleles and exhibit characteristic drug-response phenotypes[15]. We first electroporated the donor plasmid p*crt*^{Dd2}-h*dhfr* and applied WR99210 to select for episomally transformed parasites (**Fig. 3a**). These parasites were then electroporated with pZFN^{crt}-*bsd*, and blasticidin was applied for 6 d to enable transient ZFN expression and consequent homology-directed repair. Prolonged selection for the ZFN plasmid (12 d) caused a delay in parasite re-emergence after electroporation (data not shown), potentially due to repeated chromosome cleavage. After removal of blasticidin, but not WR99210, parasite proliferation was detected microscopically after 13–16 d. In a clonal analysis, we observed replacement events in 13 of 82 (15.9%) 106/1 clones and 4 of 83 (4.8%) GC03 clones by PCR (**Fig. 3b**). Southern blotting of two representative clones (GC03$^{crt\text{-}Dd2\ G9}$ and GC03$^{crt\text{-}Dd2\ H6}$) demonstrated acquisition of the donor-provided CQR *pfcrt* allele (**Fig. 3c**). We confirmed the CQ resistance phenotype of these two clones, which both displayed a four- to fivefold shift in CQ half-maximal inhibitory concentration (IC_{50}) values compared to the GC03 parent (**Fig. 3d**). Notably, in three independent transfections, 106/1 and GC03 parasites that only received the *pfcrt* donor plasmid but not the ZFN plasmid failed to yield allelic replacement parasites after more than 6 months.

Site-specific editing of a parasite drug-resistance locus

We next assessed whether our engineered *pfcrt*-targeted ZFNs could drive a subtle gene-editing event that delivers a single point mutation to the targeted site from an episomal donor template. In contrast, conventional allelic exchange strategies for *P. falciparum* typically result in significant modification of the endogenous locus by crossover-mediated incorporation of the entire plasmid (often as a concatamer), including a selectable marker and other sequence elements[3].

To achieve gene editing in *P. falciparum*, we exploited the CQ resistance–conferring properties of mutant *pfcrt*. PfCRT mediates resistance by transporting CQ from the digestive vacuole when residue Lys76 has mutated to threonine (in the case of field isolates) or isoleucine (observed in CQ-pressured 106/1 parasites[15,22,23]). *pfcrt* alleles from CQR parasite strains also possess at least three additional, potentially compensatory mutations[24]. For this experiment, we chose the CQS 106/1 strain, whose *pfcrt* allele encodes six out of seven CQR mutations observed in Asian and African strains while retaining the CQS Lys76 codon (**Fig. 4a**). On the basis of prior studies[15,22], mutation of *pfcrt* codon 76 from lysine to isoleucine in this isolate was predicted to confer resistance.

We generated the ZFN expression plasmid pZFN^{crt}-*bsd* with a 1-kb *pfcrt* donor sequence that spans the ZFN cleavage site and encodes the K76I mutation (yielding the plasmid pZFN^{crt}-76I) (**Fig. 4a**). We tested two versions of the donor sequence: one with an intact ZFN binding site ('mut1') and another with four silent mutations ('mut2'). The latter was designed to prevent ZFN binding

© 2012 Nature America, Inc. All rights reserved.

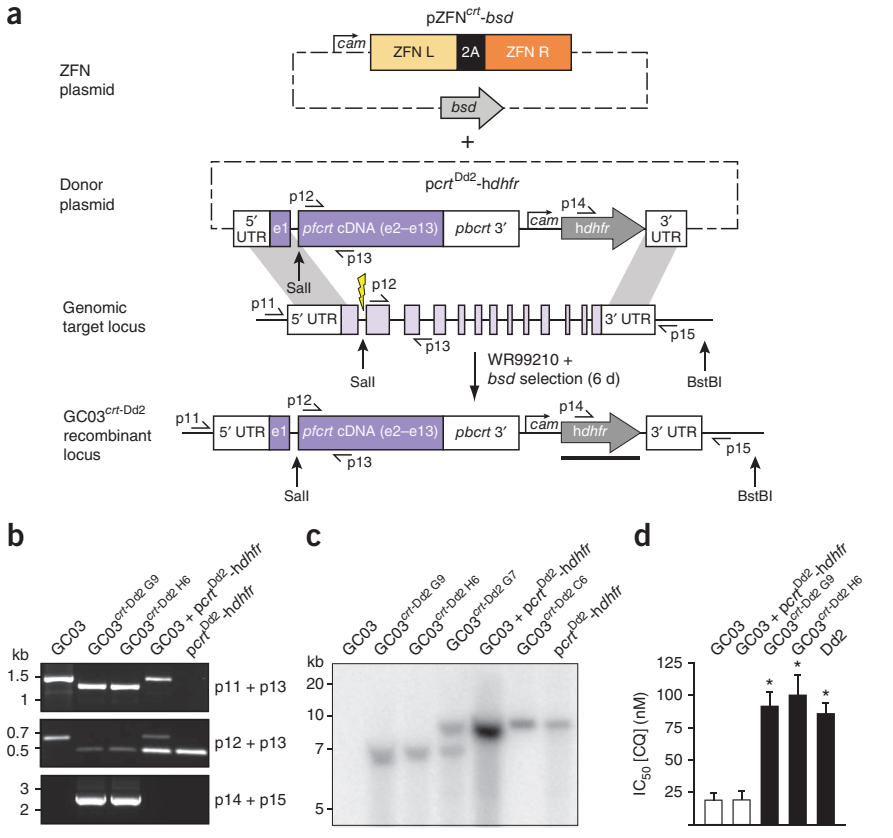

Figure 3 | ZFN-driven allelic replacement of *pfcrt*. (**a**) Schematic of the *pfcrt* allelic replacement strategy. The pZFN^{crt}-*bsd* plasmid encodes *pfcrt*-specific ZFNs, with expression driven by the *calmodulin* promoter (*cam*). The p*crt*^{Dd2}-h*dhfr* donor plasmid contains the 1.2-kb coding sequence of the Dd2 *pfcrt* allele (comprising exon 1, intron 1 and exons 2–13) followed by 0.7 kb of the *pbcrt* 3′ UTR and the h*dhfr* selectable marker (gray). These cassettes are flanked by homology regions comprising 1 kb of the *pfcrt* 3′ UTR and 0.4 kb upstream of the DSB. ZFN-driven homology-directed repair yielded the *pfcrt*-modified GC03$^{crt\text{-}Dd2}$ locus. (**b**) PCR analysis of two independent clones. Primer (p) positions are shown in **a**. (**c**) Southern blotting of genomic DNA from the indicated parasite lines digested with SalI and BstBI and probed for h*dhfr* (black bar in **a**). The band size (6.7 kb) observed with clones G9 and H6 is consistent with *pfcrt* replacement. The p*crt*^{Dd2}-h*dhfr* plasmid was linearized with SpeI (8.1 kb) and is present as episomes in clones G7 and C6 as well as in the ZFN-negative control line, GC03 + p*crt*^{Dd2}-h*dhfr*. (**d**) Plot showing half-maximal inhibitory concentration (IC_{50} ± s.e.m.) values for the indicated parasite lines. Asterisks indicate significant differences between the GC03 parental line and each of the two representative *pfcrt* allelic replacement clones GC03$^{crt\text{-}Dd2\ G9}$ and GC03$^{crt\text{-}Dd2\ H6}$ and the CQ-resistant Dd2 line (*P = 0.0286, Mann-Whitney U test, two-tailed, n = 4).

and cleavage of a successfully modified chromosomal target, thereby potentially enhancing editing efficiency. We placed 106/1 parasites under 33 nM CQ 1 d after electroporation to eliminate unmodified CQS parasites. Parasite proliferation was detected microscopically 16–33 d after electroporation. In contrast, similar CQ exposure of six independent nontransfected 106/1 cultures yielded no parasites after 90 d.

In five independent parasite transfections, we observed 100% K76I conversion rates by sequence analysis of the *pfcrt* locus (**Fig. 4a** and **Table 1**). No alternate mutations were detected at this position. Editing of the Lys76 codon was equally successful using either ZFN pair (13/15 or 14/15; **Supplementary Table 2**), irrespective of whether the ZFN binding site was mutated in the donor construct (**Table 1**). Of note, the additional four silent mutations in the mut2 template were always incorporated at the *pfcrt* locus. In addition, both the mut1 and mut2 donor templates contained a *pfcrt* 5′ UTR sequence harboring a single-base-pair deletion (a string of seven thymidines (T_7), compared to eight (T_8) in the endogenous locus). This deletion, located ~300 bp upstream of the ZFN cut site, was transferred into the edited gene sequence with a mean efficiency of 51% (**Table 1**). By comparison, mutations located an equivalent distance from the nuclease cleavage site have been captured with considerably lower frequency in mammalian cells (for example, 5% in mouse embryonic stems cells[25]). Importantly, the T_7 deletion was captured despite its presence on the side opposite the DSB relative to the selected K76I mutation (located 140 bp downstream of the ZFN cleavage site). The incorporation into the chromosomal target of all mutations on the donor plasmid could be explained by gene editing proceeding via synthesis-dependent strand annealing or other noncrossover events (**Fig. 4a** and **Supplementary Fig. 2**)[10].

We confirmed the CQ-resistance phenotype of two gene-edited lines, 106/1$^{13/15mut2}$ and 106/1$^{14/15mut1}$ (**Fig. 4b**). Both lines displayed a five- to sixfold shift in CQ IC_{50} values relative to the 106/1 parental strain. This shift in drug response was comparable to a CQR mutant of 106/1 (termed 106/1^{I76}) bearing the K76I mutation derived by CQ pressure[15,22].

Whole-genome sequencing revealed no detectable off-target activity of the *pfcrt*-targeting ZFN pairs in two representative recombinant lines (106/1$^{13/15mut1}$ and 106/1$^{14/15mut1}$). Illumina next-generation sequencing yielded a 15× coverage for >97% of all three genomes (**Supplementary Table 1**). We found no evidence of any rearrangement of the *pfcrt* locus in these edited lines, and we confirmed 100% incorporation of the K76I mutation (**Supplementary Fig. 1c**).

To demonstrate the applicability of ZFNs for generating single-nucleotide polymorphisms (SNPs) that may not confer a selectable phenotype, we repeated the ZFN-mediated *pfcrt* K76I editing event described above without applying CQ pressure. To select for transfected parasites and ensure ZFN expression, we added the h*dhfr* selection cassette to the mut2 version of the pZFN^{crt}-76I plasmid (yielding pZFN^{crt}-76I-h*dhfr*) (**Fig. 4a**). Transfected Dd2 parasites were selected with WR99210 for 6 d, and parasite proliferation was observed 11 d after removal of drug. From two independent experiments, we generated a total of 76 clones and used these to PCR-amplify the *pfcrt* genomic locus (**Table 1**). This analysis identified the ZFN binding-site mutations in 18.4% and the K76I mutation in 15.8% of clones. The upstream T_7 deletion was also found in all edited clones. These data suggest that nonselected gene-editing events can be generated efficiently enough to readily permit the isolation of modified parasite clones by limiting dilution, thus expanding the range of potential targets beyond those related to drug resistance.

© 2012 Nature America, Inc. All rights reserved.

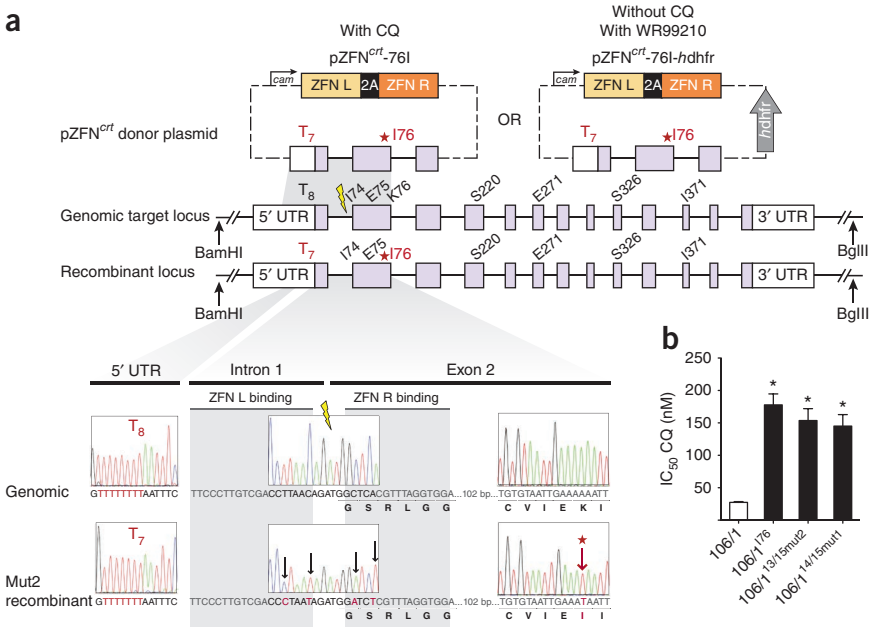

Figure 4 | ZFN editing of *pfcrt* with and without CQ selection. (**a**) Schematic of the *pfcrt* editing strategy. The *calmodulin* promoter drives expression of the *pfcrt*-specific ZFN pairs from plasmids with (pZFN^{crt}-76I-h*dhfr*) or without (pZFN^{crt}-76I) the selectable marker h*dhfr*. The homologous donor sequence for DSB repair comprises a fragment of *pfcrt* stretching 0.4 kb upstream and 0.6 kb downstream of the ZFN target site (thunderbolt). One version of the donor (termed mut1) is identical to the genomic locus but contains the mutant I76 codon (starred) that confers CQ resistance as well as a single-nucleotide deletion, T_7 (versus T_8), in the endogenous 5′ UTR. An alternate donor construct (mut2, not shown) is mutated at the ZFN binding site. Homology-dependent repair of a ZFN-induced DSB leads to incorporation of donor-provided SNPs. The chromatograms show sequence analysis of genomic and mut2 recombinant DNA. The 5′ UTR deletion as well as the mutations at the ZFN binding site and the CQ resistance–conferring I76 codon are indicated. (**b**) Plot showing half-maximal inhibitory concentration (IC_{50} ± s.e.m.) values for the indicated parasite lines. The asterisk indicates that the 106/1 parental line is significantly different (*P < 0.0286, Mann-Whitney U test, n = 4, two-tailed) from the gene-edited parasites as well as the previously established CQR line 106/1^{I76}.

DISCUSSION

Here we have established diverse ZFN-driven strategies with broad utility for interrogating the *P. falciparum* genome. These include gene disruption and replacement approaches that can be used to verify the essentiality of parasite genes as well as site-specific editing approaches to probe gene function. ZFN-mediated genome editing of *P. falciparum* differs fundamentally from prior methods of genetic manipulation, which have typically relied on stochastic integration of plasmids designed for gene disruption or allelic exchange via homologous recombination (**Supplementary Fig. 2**)[26]. In these cases, integration likely takes place after a rare and random DSB occurs in the gene of interest. Plasmid integration is typically observed after 2–4 months, and any fitness costs resulting from genome manipulation jeopardize the acquisition of the recombinant line. Extreme cases include the engineering of the *pfcrt* CQ-resistance locus, which required two rounds of genetic manipulation and over 18 months of continuous culture to obtain the desired clones[18]. Furthermore, the nondirected nature of this earlier method of allelic exchange meant that integration could take place at any genomic site with homology to the transfection plasmid, often yielding undesired outcomes. Even if integration occurs in the desired locus, single-site crossovers could result in a recombinant locus that harbors the plasmid-borne mutations in a nonfunctional duplicated fragment and not the functional gene[27].

With the approaches we describe, parasites carrying the desired specific editing event can be obtained rapidly and with an efficiency that approaches 100% in cases when the outcome yields a selectable phenotype. Notably, we could readily obtain parasites with gene-deletion, allelic-exchange or single-nucleotide editing events even in the absence of a selectable phenotype. The efficiencies of these editing events ranged from relatively high in the case of the *egfp-mrfp* replacement (88%), when ~3-kb homology arms were provided on either side of the target locus, to more modest levels (~18% efficiency) for the *pfcrt* K76I editing, when a 1-kb sequence was used as the donor template. These editing efficiencies

Table 1 | Efficiency of ZFN-mediated gene editing of *pfcrt* either with or without selection

					Proportion of editing events across sites		
	Strain	ZFN pair	Donor	Sequences analyzed	ZFN binding site	K76I	T (deletion)
CQ	106/1	13/15	*pfcrt*-76I-mut1	29 pGEM-T	N/A	29 of 29	0 of 29
	106/1	13/15	*pfcrt*-76I-mut2	25 pGEM-T	25 of 25	25 of 25	9 of 25
	106/1	14/15	*pfcrt*-76I-mut1	38 pGEM-T	N/A	38 of 38	38 of 38
	106/1	14/15	*pfcrt*-76I-mut1	28 pGEM-T	N/A	28 of 28	28 of 28
	106/1	14/15	*pfcrt*-76I-mut2	31 pGEM-T	31 of 31	31 of 31	6 of 31
	Targeting efficiency with CQ selection				100%	100%	51%
No CQ	Dd2	13/15	p*crt*-76I-mut2	36 parasite clones	4 of 36	2 of 36	4 of 4[a]
	Dd2	14/15	p*crt*-76I-mut2	40 parasite clones	10 of 40	10 of 40	10 of 10[a]
	Targeting efficiency without CQ selection				18.4%	15.8%	(18.4%)
	Distance from ZFN cut site				3–6 bp	140 bp	296 bp

The table shows ZFN-mediated *pfcrt* gene-targeting efficiency in the presence or absence of CQ pressure. The site of cleavage of the ZFN pairs and constructs are described in **Figure 4**.
[a]Only lines identified as edited at the binding site were analyzed with a second sequencing reaction for the T (deletion).

© 2012 Nature America, Inc. All rights reserved.

were sufficient to readily isolate parasite clones bearing the desired modifications. Furthermore, the capture of mutations several hundred base pairs from the DSB site provides some flexibility when selecting ZFN pairs. The shortest region of homology was 0.5 kb (for the *egfp* disruption strategy), and the potential increase in editing efficiency by using longer regions must be balanced by constraints on the size and stability in *E. coli* of AT-rich *P. falciparum* transfection plasmids.

ZFN-mediated editing can now be leveraged to generate knockouts or more subtle modifications (including fusions with fluorescent reporters[20] or affinity tags) that probe parasite gene function across a broad range of biological contexts. This includes the ability to inactivate genes without integrating a selectable marker, thus fulfilling an important requirement for genetically attenuated vaccines. ZFNs can also be deployed for sequence-specific editing[28]—for example, to assess the involvement of candidate loci and identify causal polymorphisms in order to survey the spread of antimalarial drug resistance in endemic areas. ZFN-mediated genome editing now adds a powerful reverse-genomic methodology for dissecting the etiologic agent of a major human infectious disease.

METHODS

Methods and any associated references are available in the online version of the paper.

Requests for materials. Requests for ZFNs should be directed to furnov@sangamo.com.

Note: Supplementary information is available in the online version of the paper.

ACKNOWLEDGMENTS

We thank L. Symington (Columbia University) for helpful discussions, and the sequencing core facility and staff in the Lewis-Sigler Institute for Integrative Genomics at Princeton University. M.L. is funded by a US National Institutes of Health Director's New Innovators Award (1DP2OD001315) and receives support from the Center for Quantitative Biology (P50 GM071508). D.A.F. gratefully acknowledges support from the US National Institutes of Health (R01 AI50234 and AI079709).

AUTHOR CONTRIBUTIONS

J.S., M.C.S.L., B.Z., A.H.L., M.L., F.D.U. and D.A.F. designed the experiments, which were performed by J.S., M.C.S.L., A.H.L. and A.E.W. B.Z., J.R.P., L.Z., E.J.R., P.D.G. and F.D.U. designed and provided the zinc-finger nucleases. J.S., M.C.S.L., A.H.L., F.D.U. and D.A.F. wrote the manuscript, with input from all authors.

COMPETING FINANCIAL INTERESTS

The authors declare competing financial interests: details are available in the online version of the paper.

Published online at http://www.nature.com/doifinder/10.1038/nmeth.2143. Reprints and permissions information is available online at http://www.nature.com/reprints/index.html.

1. Dondorp, A.M. *et al.* The threat of artemisinin-resistant malaria. *N. Engl. J. Med.* **365**, 1073–1075 (2011).
2. Meissner, M., Breinich, M.S., Gilson, P.R. & Crabb, B.S. Molecular genetic tools in *Toxoplasma* and *Plasmodium*: achievements and future needs. *Curr. Opin. Microbiol.* **10**, 349–356 (2007).
3. Anderson, T., Nkhoma, S., Ecker, A. & Fidock, D. How can we identify parasite genes that underlie antimalarial drug resistance? *Pharmacogenomics* **12**, 59–85 (2011).
4. Bibikova, M., Golic, M., Golic, K.G. & Carroll, D. Targeted chromosomal cleavage and mutagenesis in *Drosophila* using zinc-finger nucleases. *Genetics* **161**, 1169–1175 (2002).
5. Carroll, D. Genome engineering with zinc-finger nucleases. *Genetics* **188**, 773–782 (2011).
6. Miller, J.C. *et al.* An improved zinc-finger nuclease architecture for highly specific genome editing. *Nat. Biotechnol.* **25**, 778–785 (2007).
7. Doyon, Y. *et al.* Enhancing zinc-finger-nuclease activity with improved obligate heterodimeric architectures. *Nat. Methods* **8**, 74–79 (2011).
8. Urnov, F.D. *et al.* Genome editing with engineered zinc finger nucleases. *Nat. Rev. Genet.* **11**, 636–646 (2010).
9. Gardner, M.J. *et al.* Genome sequence of the human malaria parasite *Plasmodium falciparum*. *Nature* **419**, 498–511 (2002).
10. Mimitou, E.P. & Symington, L.S. DNA end resection: many nucleases make light work. *DNA Repair (Amst.)* **8**, 983–995 (2009).
11. Szymczak, A.L. *et al.* Correction of multi-gene deficiency *in vivo* using a single 'self-cleaving' 2A peptide-based retroviral vector. *Nat. Biotechnol.* **22**, 589–594 (2004).
12. Adjalley, S.H. *et al.* Quantitative assessment of *Plasmodium falciparum* sexual development reveals potent transmission-blocking activity by methylene blue. *Proc. Natl. Acad. Sci. USA* **108**, E1214–E1223 (2011).
13. Fidock, D.A., Nomura, T. & Wellems, T.E. Cycloguanil and its parent compound proguanil demonstrate distinct activities against *Plasmodium falciparum* malaria parasites transformed with human dihydrofolate reductase. *Mol. Pharmacol.* **54**, 1140–1147 (1998).
14. Deitsch, K., Driskill, C. & Wellems, T. Transformation of malaria parasites by the spontaneous uptake and expression of DNA from human erythrocytes. *Nucleic Acids Res.* **29**, 850–853 (2001).
15. Fidock, D.A. *et al.* Mutations in the *P. falciparum* digestive vacuole transmembrane protein PfCRT and evidence for their role in chloroquine resistance. *Mol. Cell* **6**, 861–871 (2000).
16. Bray, P.G. *et al.* Defining the role of PfCRT in *Plasmodium falciparum* chloroquine resistance. *Mol. Microbiol.* **56**, 323–333 (2005).
17. Summers, R.L., Nash, M.N. & Martin, R.E. Know your enemy: understanding the role of PfCRT in drug resistance could lead to new antimalarial tactics. *Cell. Mol. Life Sci.* **69**, 1967–1995 (2012).
18. Sidhu, A.B.S., Verdier-Pinard, D. & Fidock, D.A. Chloroquine resistance in *Plasmodium falciparum* malaria parasites conferred by *pfcrt* mutations. *Science* **298**, 210–213 (2002).
19. Valderramos, S.G. *et al.* Identification of a mutant PfCRT-mediated chloroquine tolerance phenotype in *Plasmodium falciparum*. *PLoS Pathog.* **6**, e1000887 (2010).
20. Doyon, J.B. *et al.* Rapid and efficient clathrin-mediated endocytosis revealed in genome-edited mammalian cells. *Nat. Cell Biol.* **13**, 331–337 (2011).
21. Doyon, Y. *et al.* Heritable targeted gene disruption in zebrafish using designed zinc-finger nucleases. *Nat. Biotechnol.* **26**, 702–708 (2008).
22. Cooper, R.A. *et al.* Alternative mutations at position 76 of the vacuolar transmembrane protein PfCRT are associated with chloroquine resistance and unique stereospecific quinine and quinidine responses in *Plasmodium falciparum*. *Mol. Pharmacol.* **61**, 35–42 (2002).
23. Martin, R.E. *et al.* Chloroquine transport via the malaria parasite's chloroquine resistance transporter. *Science* **325**, 1680–1682 (2009).
24. Sá, J.M. *et al.* Geographic patterns of *Plasmodium falciparum* drug resistance distinguished by differential responses to amodiaquine and chloroquine. *Proc. Natl. Acad. Sci. USA* **106**, 18883–18889 (2009).
25. Elliott, B. *et al.* Gene conversion tracts from double-strand break repair in mammalian cells. *Mol. Cell. Biol.* **18**, 93–101 (1998).
26. Carvalho, T.G. & Menard, R. Manipulating the *Plasmodium* genome. *Curr. Issues Mol. Biol.* **7**, 39–55 (2005).
27. Sidhu, A.B.S., Valderramos, S.G. & Fidock, D.A. *pfmdr1* mutations contribute to quinine resistance and enhance mefloquine and artemisinin sensitivity in *Plasmodium falciparum*. *Mol. Microbiol.* **57**, 913–926 (2005).
28. Urnov, F.D. *et al.* Highly efficient endogenous human gene correction using designed zinc-finger nucleases. *Nature* **435**, 646–651 (2005).

© 2012 Nature America, Inc. All rights reserved.

ONLINE METHODS

Zinc-finger nuclease engineering. ZFNs specific for *egfp* have been described previously[29]. ZFNs targeting *pfcrt* (MAL7P1.27) were designed and assembled using an archive of validated modules[8] and screened for activity using a yeast proxy system[21].

Plasmid construction. To test whether the *Thosea asigna* virus 2A peptide[11] could mediate cotranslational polypeptide separation in *P. falciparum*, we generated the pDC2-*cam*-*mrfp*-2A-*gfp*-attP plasmid (whose expression cassette is illustrated in **Fig. 1a**). The 2A and *mrfp* fragments were first amplified separately and linked by 'splicing by overlap extension' (SOE) PCR. The 2A sequence was amplified from the plasmid pVAX-ZFN-L-2A-ZFN-R[21] using primers p18 + p19 (**Supplementary Table 3**), and *mrfp* was amplified from pML2 (ref. 30) using primers p21 + p22. The linked *mrfp*-2A sequence was amplified using primer p21 and either p19 (full 2A sequence) or p20 (2AΔP21). Finally, the *mrfp*-2A fusions were digested with AvrII and BglII and inserted into a pDC2-based expression vector[30] following excision of the 5′ *gfp* full-length sequence in the tandem *gfp*-*gfp* plasmid pDC2-*cam*-*gfp*(N-C)-attP. To generate the construct used to produce the NF54^{EGFP} line, the *egfp* coding sequence was amplified from an EGFP-FokI plasmid using primers p23 + p24 and was cloned into the AvrII and XhoI restriction sites of pDC2-*cam*-*gfp*(N-C)-attP. This cloning yielded the *egfp* integration plasmid pDC2-*cam*-*egfp*-attP used to generate the NF54^{EGFP} line.

Expression of ZFNs in *P. falciparum* was achieved by cloning these downstream of a *calmodulin* (PF14_0323) promoter and upstream of an *hsp86* (PF07_0030) 3′ UTR in a pDC2 vector with or without the h*dhfr* or *bsd* selectable marker. ZFNs linked with the 2A peptide were digested with NheI and XhoI and were cloned into the compatible restriction sites AvrII and XhoI, thereby yielding the intermediate plasmids pZFN^{egfp} and pZFN^{crt} and the final transfection plasmids pZFN^{egfp}-h*dhfr* and pZFN^{crt}-*bsd*. The donor templates provided for the ZFN-induced DSB repair were either placed on the same plasmid as the ZFN expression cassette or on a separate plasmid, as indicated below.

To generate the *egfp*-h*dhfr* donor template (**Fig. 1b**), we first amplified 5′ and 3′ regions of homology flanking the ZFN cleavage site in the integrated *egfp* locus. The 5′ region was PCR-amplified from pDC2-*cam*-*egfp*-attP using primers p3 + p25 (yielding a 543-bp product), whereas the 3′ region (denoted *egfp* 3′) was amplified using primers p27 + p28 (yielding a 795-bp product). A promoterless h*dhfr* selection cassette was then amplified with primers p26 + p4 and fused in frame to *egfp* 5′ using primers p3 + p4 in a SOE PCR reaction. The *egfp*-h*dhfr* template was then cloned into pZFN^{egfp} using ApaI and SacII restriction sites. The second homologous region *egfp* 3′ was then inserted using the restriction sites BstAPI and ZraI, thereby yielding the transfection plasmid pZFN^{egfp}-*egfp*-h*dhfr* (**Fig. 1b**). To produce the p*egfp*-h*dhfr* control plasmid, we excised the *egfp*-specific ZFN segment following HindIII digestion of pZFN^{egfp}-*egfp*-h*dhfr* and agarose gel electrophoresis, and then we religated the plasmid.

To assemble the *mrfp*-*vps4* donor template (**Fig. 2a**), we amplified *mrfp* and *vps4* separately and then linked the two products by SOE PCR. The *mrfp* sequence was amplified from pML2 (ref. 30) using primers p29 + p30, and *vps4* was amplified from NF54 genomic DNA using primers p31 + p32. The linked *mrfp*-*vps4* sequence was amplified with p29 + p32 and cloned into the AvrII and XhoI restriction sites of pDC2, thereby yielding the replacement plasmid p*mrfp*-*vps4*.

To generate the p*crt*^{Dd2}-h*dhfr* donor plasmid for *pfcrt* allelic replacement (**Fig. 3a**), we first amplified intron 1 through exon 13 of *pfcrt* Dd2 cDNA and *pbcrt* 3′ UTR from an expression plasmid[31] using p33 + p34. The PCR product was cloned into the restriction sites NotI and SpeI of the pCC1 plasmid (containing an h*dhfr* cassette). The left homology region, comprising the *pfcrt* 5′ UTR to intron 1 sequence (431 bp), was subcloned from the pZFN^{crt}-76I plasmid with ApaI and SalI (see below). The *pfcrt* 3′ UTR served as the right region of homology and was amplified from 106/1 gDNA using primers p35 + p36 (yielding a 1,050-bp product) and then inserted into EcoRI and ClaI to generate the allelic replacement plasmid p*crt*^{Dd2}-h*dhfr* (**Fig. 3a**).

We generated two donor constructs to introduce a single point mutation (K76I) in *pfcrt*, located 140 bp downstream of the ZFN cut site. A 1-kb donor fragment without additional mutations at the ZFN target site (mut1) was PCR-amplified from genomic DNA isolated from 106/1^{I76} parasites[15] using primers p37 + p38 and was cloned into the ApaI and SacI restriction sites in pZFN^{crt}. We also generated a second donor template with four silent mutations at the ZFN binding site (mut2) via SOE PCR using primers p37 + p39 and p38 + p40 for the first round of PCR and p37 + p38 for the second round (**Supplementary Table 3**). The same restrictions sites ApaI and SacI were used to clone donor fragment mut2. Both donor constructs contained a single-nucleotide (T) deletion in the 5′ UTR of *pfcrt* located 0.3 kb upstream of the ZFN cut site. The two ZFN pairs (13/15 and 14/15; **Supplementary Table 2**) were expressed from a plasmid (pZFN^{crt}-76I) containing either the mut1 or mut2 donor.

Parasite cultures and transfections. Asexual blood-stage parasites were propagated in human red blood cells in RPMI-1640 malaria culture medium[13] with 0.5% (w/v) Albumax II (Invitrogen) under 5% O_2/5% CO_2/90% N_2. Parasites were electroporated with purified circular plasmid DNA as described[13]. The 2A test line expressing mRFP-2A-GFP (**Fig. 1a**) was generated by attB × attP crossover-mediated integration[32] of the pDC2-*cam*-*mrfp*-2A-*gfp*-attP plasmid into the *cg6* locus of the recipient line Dd2^{attB}. The NF54^{EGFP} target line (**Fig. 1b**) was similarly generated by attB × attP–mediated integration of the EGFP expression plasmid (pDC2-*cam*-*egfp*-attP) into the NF54^{attB} line[12]. attB × attP crossover events were mediated by Bxb serine integrase, which was supplied by cotransfection with the plasmid pINT[32].

To test for ZFN-mediated cleavage of our integrated *egfp* sequence, we electroporated NF54^{EGFP} parasites with the plasmid pZFN^{egfp}*egfp*-h*dhfr*. This plasmid was designed to integrate a functional *egfp*-h*dhfr* fusion (**Fig. 1b**) expressed from the upstream *calmodulin* promoter and conferring resistance to WR99210 (Jacobus Pharmaceuticals). Parasites were selected with 2.5 nM WR99210 for 24 (line A), 48 (line B1), 96 (line B2) or 120 h (line B3) after electroporation. To potentially increase the efficiency of plasmid delivery and gene disruption, lines B1–B3 were supplemented (1:1) with red blood cells preloaded with additional plasmid (50 µg) 24 h after electroporation[14]. In a control experiment, we electroporated the donor plasmid p*egfp*-h*dhfr* lacking the *egfp*-specific ZFNs and started selection

© 2012 Nature America, Inc. All rights reserved.

with 2.5 nM WR99210 the following day. All phenotypic and genotypic analyses of this set of parasite lines were performed on bulk cultures.

To perform our ZFN-driven *egfp* replacement with *mrfp*, we coelectroporated NF54^{EGFP} parasites with the plasmids pZFN^{egfp}-h*dhfr* and *pmrfp-vps4* (**Fig. 2a**). The pZFN^{egfp}-h*dhfr* plasmid contained the 2A-linked *egfp*-specific ZFNs that were expressed from a *calmodulin* promoter. Selection for this plasmid was applied with 2.5 nM WR99210, which was applied 1 d post-electroporation and was maintained for 6 d. The *pmrfp-vps4* plasmid provided the *mrfp* donor sequence flanked by homologous regions. No selection was applied for this plasmid. Parasite clones illustrated in **Figure 2** were generated by limiting dilution.

To replace the endogenous *pfcrt* allele, GC03 and 106/1 parasites were first electroporated with the donor plasmid p*crt*^{Dd2}-h*dhfr* and selected with 2.5 nM WR99210 to enrich for episomally transformed parasites. These parasites (GCO3 + p*crt*^{Dd2}-h*dhfr* or 106/1 + p*crt*^{Dd2}-h*dhfr*) were then electroporated with pZFN^{crt}-*bsd* (**Fig. 3a**). One day after electroporation, parasites were selected with 2 μg/ml blasticidin (Invitrogen) and 2.5 nM WR99210 for 6 d and then selected with only WR99210. Parasite clones were generated by limiting dilution where indicated.

To edit *pfcrt* using CQ selection, 106/1 parasites were electroporated with pZFN^{crt}-76I plasmids harboring either the mut1 or mut2 sequence template (the latter harbored four ZFN binding site mutations). Transformed parasites were treated with 33 nM CQ phosphate (Sigma-Aldrich) to select for acquisition of the K76I mutation (**Fig. 4a**). To edit *pfcrt* without CQ selection, Dd2 parasites were electroporated with pZFN^{crt}-76I-h*dhfr*. One day after electroporation, parasites were exposed to 2.5 nM WR99210 for 6 d to select for plasmid transformation (**Fig. 4a**). Analysis of parasite lines was performed on bulk cultures.

DNA analysis. *P. falciparum* trophozoite-infected erythrocytes were harvested and saponin-lysed. Parasite genomic DNA was extracted and purified using DNeasy Blood kits (Qiagen). Integration of the h*dhfr* cassette into the *cg6-egfp* locus of NF54^{EGFP} parasites was confirmed by PCR amplification of the target locus using primers p1 + p2 (yielding a 1.8-kb fragment), p1 + p4 (3.9 kb), p5 + p7 (4.2 kb) and p3 + p6 (1.5 kb in NF54^{EGFP} and 3.4 kb in ZFN-transfected parasites) (**Fig. 1b**,**d**). Replacement of the integrated *egfp* with *mrfp* at the chromosomal *cg6* locus was shown by PCR amplification of the target locus using primers p10 + p7 (yielding a 5.7-kb fragment), p1 + p9 (yielding a 4.8-kb fragment) and p8 + p6 (yielding a 2.8-kb fragment for the *mrfp-vps4* replacement, compared with 1.6 kb for the original *egfp* locus and 3.3 kb for the *zfn* cassette) (**Fig. 2a**,**d**).

Allelic replacement of the endogenous GC03 *pfcrt* locus by the p*crt*^{Dd2}-h*dhfr* donor sequence was confirmed by PCR of the target locus with primers p11 + p13 (GC03 parent: 1.4 kb, GC03$^{crt\text{-}Dd2}$ recombinant: 1.2 kb, GC03 + p*crt*^{Dd2}-h*dhfr*: 1.4 kb, p*crt*^{Dd2}-h*dhfr*: no product); p12 + p13 (GC03: 0.6 kb, GC03$^{crt\text{-}Dd2}$: 0.4 kb, GC03 + p*crt*^{Dd2}-h*dhfr*: 0.4 and 0.6 kb, p*crt*^{Dd2}-h*dhfr*: 0.4 kb); and p14 + p15 (GC03: no product, GC03$^{crt\text{-}Dd2}$: 2.5 kb, GC03 + p*crt*^{Dd2}-h*dhfr*: no product, p*crt*^{Dd2}-h*dhfr*: no product) (**Fig. 3a**,**c**).

Editing of *pfcrt* codon 76 (**Fig. 4**) was confirmed by PCR-amplifying the genomic locus with primers p23 + p27 that flank the *pfcrt* donor sequence. These products were amplified either from bulk cultures (and afterward cloned into pGEM-T), or from parasite clones (**Table 1**). Sequencing was performed with primers p24, p25, p26, p18 and p20 (**Supplementary Table 3**).

Whole-genome sequencing and data processing. Genomic DNA was prepared from the parental line NF54^{EGFP} and the two ZFN-transfected lines NF54$^{\Delta egfpA}$ and NF54$^{\Delta egfpB1}$ as well as from 106/1 and 106/1$^{13/15mut1}$ and 106/1$^{14/15\ mut1}$. These DNAs were sheared (10 μg per line) to obtain a fragment size of ~200–400 bp using an E220 focused-ultrasonicator (Covaris Inc.) and the following settings: 10% duty cycle, intensity 5, 200 cycles per burst, 180 s treatment time. Sheared gDNA was size selected on a 2% low-melting agarose gel and then purified. Barcoded libraries for Illumina TruSeq single-end sequencing were then constructed from the size-selected, sheared material using NEBNext DNA Library Preparation reagents (NEB) by following the standard Illumina library preparation protocol but omitting the final size-selection step. To assess the quality and percentage of adaptor-ligated material, the final sequencing libraries were tested on an Agilent 2100 Bioanalyzer (Agilent Technologies) along with the original size-selected fragmented gDNA from the same preparation. The concentration of each library was determined using a Quant-iT dsDNA Broad-Range Assay Kit (Invitrogen). For the NF54$^{\Delta egfpB1}$ line, the sequencing adaptor ligation was determined to be less than 50% efficient. We therefore PCR-amplified the sequencing library as described[33] to minimize GC bias. PCR conditions for 50-μl reactions were: 1× Kapa HiFi Buffer, 60 nM tetramethylammonium chloride, 0.3 mM each dNTP, 0.4 μM each primer and 1 U Kapa HiFi DNA polymerase, with thermocycling conditions of 1 min at 98 °C followed by 12 cycles of 10 s at 98 °C, 1 min at 55 °C and finally 5 min at 55 °C. The final libraries were multiplexed with three barcoded samples and 20% PhiX control DNA per lane and were sequenced using an Illumina HiSeq 2000 system.

Sequencing outputs were uploaded into Galaxy[34], which is hosted locally at the Lewis-Sigler Institute for Integrative Genomics at Princeton University. Sequence reads were mapped to the *P. falciparum* 3D7 reference genome v. 8.0 (http://plasmodb.org/common/downloads/release-8.0/Pfalciparum/) using the Burrows-Wheeler alignment tool[35], and files were formatted using Sequence Alignment/Maptools[36]. GATK tools were applied to assess depths of coverage for the overall genomes and specific regions of interest and to perform SNP discovery and filtering using standard hard-filtering parameters[37]. Alignments and variants were visualized using the Integrative Genomics Viewer[38].

Southern blot hybridizations. Edited lines obtained from the *egfp* disruption and the *egfp*/*mrfp* replacement experiments and the parental control were analyzed using pairs of Southern blots, as follows. For each blot, 2 μg of genomic DNA was digested with ClaI + BamHI, separated by electrophoresis on a 0.7% agarose gel and transferred onto a Nytran nylon membrane. Hybridization of the first blot was performed at 54 °C with a 710-bp ^{32}P-labeled *egfp* probe that was PCR-amplified from pDC2-*cam-egfp*-attP using primers p3 + p26. The second blot was either hybridized with a 560-bp ^{32}P-labeled h*dhfr* probe or a 670-bp ^{32}P-labeled *mrfp* probe amplified by PCR with primers p10 + p17 (*mrfp*) or p28 + p4 (h*dhfr*) from the respective plasmids p*mrfp-vps4* or pZFN^{egfp}-h*dhfr*. Linearized transfection plasmids served as positive controls (8.4 kb, 8.3 kb and 9.9 kb for the *egfp*, *mrfp* and h*dhfr* experiment, respectively; see **Figs. 1e** and **2e**).

© 2012 Nature America, Inc. All rights reserved.

doi:10.1038/nmeth.2143

Parasite lines obtained following *pfcrt* allelic replacement were analyzed on pairs of Southern blots, for which 2 µg of genomic DNA was digested with SalI + BstBI. Digests were separated by electrophoresis on a 0.7% agarose gel and transferred onto a Nytran nylon membrane. Hybridization was performed at 55 °C with a 600-bp ^{32}P-labeled h*dhfr* probe amplified from p*crt*^{Dd2}-h*dhfr* by PCR with primers p26 + p4.

***In vitro* susceptibility assays.** *In vitro* IC_{50} values were determined by incubating parasites for 72 h across a range of concentrations of CQ (2,000 nM –2.5 nM). After 72 h of incubation, parasite growth was determined by measuring parasitemia using flow cytometry. Cells were stained with 1.6 µM Mito Tracker Deep Red and 2× SYBR Green (Invitrogen) in 1× PBS supplemented with 5% FBS[39]. *In vitro* IC_{50} values were calculated by nonlinear regression analysis and Mann-Whitney *U* tests were used for statistical analysis. A nonparametric statistical analysis was appropriate as experiments were independent and no normal distribution was assumed.

For the *pfcrt* gene-replacement experiment (**Fig. 3d**), the IC_{50} value for the GC03 parental line (mean ± s.e.m. 18.4 ± 5.3 nM, $n = 4$) was significantly different from the two *pfcrt* allelic replacement clones GC03$^{crt\text{-}Dd2\ G9}$ (91.8 ± 10.7 nM, $n = 4$, $P = 0.028$, two-tailed) and GC03$^{crt\text{-}Dd2\ H6}$ (100.3 ± 15.5 nM, $n = 4$, $P = 0.028$, two-tailed). No significant difference in IC_{50} values was observed between the parental GCO3 line and the control GC03 + p*crt*^{Dd2}-h*dhfr* line that episomally replicated the donor plasmid (18.6 ± 6.8 nM, $n = 4$, $P = 1.0$, two-tailed).

For the *pfcrt* gene-editing experiment (**Fig. 4b**), the IC_{50} value for the 106/1 parental line (mean ± s.e.m. 27.4 ± 1.2 nM, $n = 4$) was significantly different (*$P = 0.028$, two-tailed, Mann-Whitney *U* test) from the gene-edited parasites 106/1$^{13/15mut2}$ (153.6 ± 18.3 nM) and 106/1$^{14/15mut1}$ (145.1 ± 17.8 nM) as well as the previously established CQR line 106/1^{I76} (177.9 ± 16.8 nM).

Fluorescence analysis of recombinant parasites. For live-cell imaging, resuspended cultures were washed once with RPMI-1640 media lacking Albumax II, and the cells were applied to poly(L-lysine)-coated glass-bottom culture dishes (MatTek) and overlaid with 1 ml of RPMI media containing 2 µg/ml Hoechst 33342 (Sigma) to stain the nuclei. Images were acquired on a Nikon Ti-E inverted microscope with 100× N.A. 1.4 PlanApo optics and a CoolSnap HQ2 camera. Images were collected with Nikon NIS Elements software and assembled using Adobe Photoshop.

To quantify the proportion of EGFP-positive parasites in the NF54^{EGFP} and ZFN-modified lines, parasite cultures were analyzed by flow cytometry. Cells were stained for 10 min with 250 nM SYTO 61 dye (Invitrogen) in aqueous solution containing 0.2% dextrose and 0.9% sodium chloride. After a single wash, 50,000 cells were counted on an Accuri C6 Flow Cytometer. Data were analyzed with FlowJo 7.6.3 with gating for nuclear stain SYTO 61 (FL4) and for green fluorescence (FL1).

29. Geurts, A.M. *et al.* Knockout rats via embryo microinjection of zinc-finger nucleases. *Science* **325**, 433 (2009).
30. Lee, M.C., Moura, P.A., Miller, E.A. & Fidock, D.A. *Plasmodium falciparum* Sec24 marks transitional ER that exports a model cargo via a diacidic motif. *Mol. Microbiol.* **68**, 1535–1546 (2008).
31. Ecker, A. *et al.* Evidence that mutant PfCRT facilitates the transmission to mosquitoes of chloroquine-treated *Plasmodium* gametocytes. *J. Infect. Dis.* **203**, 228–236 (2011).
32. Nkrumah, L.J. *et al.* Efficient site-specific integration in *Plasmodium falciparum* chromosomes mediated by mycobacteriophage Bxb1 integrase. *Nat. Methods* **3**, 615–621 (2006).
33. Oyola, S.O. *et al.* Optimizing Illumina next-generation sequencing library preparation for extremely AT-biased genomes. *BMC Genomics* **13**, 1 (2012).
34. Goecks, J., Nekrutenko, A. & Taylor, J. Galaxy: a comprehensive approach for supporting accessible, reproducible, and transparent computational research in the life sciences. *Genome Biol.* **11**, R86 (2010).
35. Li, H. & Durbin, R. Fast and accurate short read alignment with Burrows-Wheeler transform. *Bioinformatics* **25**, 1754–1760 (2009).
36. Li, H. *et al.* The Sequence Alignment/Map format and SAMtools. *Bioinformatics* **25**, 2078–2079 (2009).
37. DePristo, M.A. *et al.* A framework for variation discovery and genotyping using next-generation DNA sequencing data. *Nat. Genet.* **43**, 491–498 (2011).
38. Robinson, J.T. *et al.* Integrative genomics viewer. *Nat. Biotechnol.* **29**, 24–26 (2011).
39. Ekland, E.H., Schneider, J. & Fidock, D.A. Identifying apicoplast-targeting antimalarials using high-throughput compatible approaches. *FASEB J.* **25**, 3583–3593 (2011).

© 2012 Nature America, Inc. All rights reserved.